

Probing $\Omega\Omega$ and $p\Omega$ dibaryons with femtoscopic correlations in relativistic heavy-ion collisionsKenji Morita ^{1,2,3,*}, Shinya Gongyo,¹ Tetsuo Hatsuda ^{4,1}, Tetsuo Hyodo,^{5,6} Yuki Kamiya ⁷ and Akira Ohnishi ^{5,†}¹*RIKEN Nishina Center, Wako 351-0198, Japan*²*Institute of Theoretical Physics, University of Wrocław, PL-50204, Wrocław, Poland*³*National Institutes for Quantum and Radiological Science and Technology, Rokkasho Fusion Institute, Rokkasho, Aomori 039-3212, Japan*⁴*RIKEN Interdisciplinary Theoretical and Mathematical Science Program (iTHEMS), Wako 351-0198, Japan*⁵*Yukawa Institute for Theoretical Physics, Kyoto University, Kyoto 606-8502, Japan*⁶*Department of Physics, Tokyo Metropolitan University, Hachioji 192-0397, Japan*⁷*CAS Key Laboratory of Theoretical Physics, Institute of Theoretical Physics, Chinese Academy of Sciences, Beijing 100190, China*

(Received 28 August 2019; published 6 January 2020; corrected 29 October 2020)

The momentum correlation functions of baryon pairs, which reflects the baryon-baryon interaction at low energies, are investigated for multistrangeness pairs ($\Omega\Omega$ and $N\Omega$) produced in relativistic heavy-ion collisions. We calculate the correlation functions based on an expanding source model constrained by single-particle distributions. The interaction potentials are taken from those obtained from recent lattice QCD calculations at nearly physical quark masses. Experimental measurements of these correlation functions for different system sizes will help to disentangle the strong interaction between baryons and to unravel the possible existence of strange dibaryons.

DOI: [10.1103/PhysRevC.101.015201](https://doi.org/10.1103/PhysRevC.101.015201)**I. INTRODUCTION**

Either bound or resonant dibaryons provide valuable information on baryon-baryon interactions [1,2]. Historic example is the bound deuteron [3] which indicates the strong tensor force in the 3SD_1 nucleon-nucleon interaction [4]. Similarly, observing possible dibaryons with multistrangeness would give useful constraints on the unknown hyperon-nucleon and hyperon-hyperon interactions. The H -dibaryon with spin $J=0$ and $S=-2$ [5], the $N\Omega$ with $J=2$ and $S=-3$ [6,7], and the $\Omega\Omega$ with $J=0$ and $S=-6$ [8] are particularly interesting, since the Pauli blocking among valence quarks do not operate in these systems.

In recent years, *ab initio* calculations of baryon-baryon interactions on the basis of lattice quantum chromodynamics (LQCD) became possible near the physical quark masses. This is due to the development of advanced techniques such as the HAL QCD (Hadron to Atomic Nuclei from Lattice QCD) method [9,10] and the unified contraction algorithm [11]. In particular, it was numerically demonstrated that the $\Omega\Omega$ interaction in the $J=0$ channel and the $N\Omega$ interaction in the $J=2$ channel are attractive enough to hold molecular-like bound states in the S -wave [12,13].

To study such multistrangeness systems experimentally, high-energy heavy-ion collisions provide a unique opportunity allowing direct search via invariant mass spectrum [14,15] as well as indirect search via momentum correlations [15–19]. As for the latter, a ratio of the correlation functions obtained from different source sizes has been theoretically

introduced and called “small-to-large ratio” (SL) [17]. This is useful to access, e.g., the strong $p\Omega$ interaction without much contamination from the Coulomb interaction at small relative momentum. Subsequently, the measurement of the momentum correlation of $p\Omega$ was conducted in Au+Au collisions at the Relativistic Heavy Ion Collider (RHIC) [20].

The main purpose of this paper is to study the pair momentum correlation functions of the dibaryon candidates, $\Omega\Omega$ and $p\Omega$, by extending our previous analysis [15–19]. We employ the latest interactions obtained from the (2+1)-flavor lattice QCD simulations with nearly physical quark masses [12,13]. Also we use an expanding source model constrained by experimental transverse-momentum spectra and multiplicities. In Sec. II, we recapitulate the general feature of the momentum correlation function in a simplified example to give an account of how the final-state interaction (FSI) is translated into the pair correlations. A model for the emission source function is described in Sec. III. We give details of the potential and resultant correlation functions for $\Omega\Omega$ pairs and $p\Omega$ pairs in Secs. IV and V, respectively. Section VI is devoted to summary and concluding remarks. In Appendix A, the system size dependence of the momentum correlation for $p\Omega$ with uncertainty quantification are examined. In Appendix B, we show a comparison of the $p\Omega$ potential in Ref. [17] with that in Ref. [13] adopted in the present paper.

II. TWO-PARTICLE MOMENTUM CORRELATION FROM FINAL-STATE INTERACTIONS**A. Formalism**

We briefly recapitulate the general property of the two-particle momentum correlation function with FSI. More details can be found in, e.g., Refs. [15,21].

*morita.kenji@qst.go.jp

†ohnishi@yukawa.kyoto-u.ac.jp

The momentum correlation function between particles 1 and 2 with respective momenta p_1 and p_2 is defined by the ratio of two-particle spectrum $N_{12}(\mathbf{p}_1, \mathbf{p}_2) = E_1 E_2 dN_{12}/d\mathbf{p}_1 d\mathbf{p}_2$ and the product of single-particle spectra $N_i(\mathbf{p}_i) = E_i dN_i/d\mathbf{p}_i$ as

$$C(q^\mu, P^\mu) = \frac{N_{12}(\mathbf{p}_1, \mathbf{p}_2)}{N_1(\mathbf{p}_1)N_2(\mathbf{p}_2)}, \quad (1)$$

with $E_i = \sqrt{\mathbf{p}_i^2 + m_i^2}$ being the on-shell particle energy. The center-of-mass momentum P and the generalized relative momentum q are defined by

$$P^\mu = p_1^\mu + p_2^\mu, \quad (2)$$

$$q^\mu = \frac{1}{2} \left[p_1^\mu - p_2^\mu - \frac{(p_1 - p_2)P}{P^2} P^\mu \right]. \quad (3)$$

One may, in principle, measure the correlation function as a function of three independent components of the relative momentum q^μ . Such a decomposition has been utilized to investigate expansion dynamics of the hot matter through pion correlations [21]. In practice, particles except for pions do not allow for such detailed study due to limited statistics. Hereafter, we consider only one-dimensional correlation function with respect to the invariant relative momentum $q = \sqrt{-q_\mu q^\mu}$. Then we can define the experimental correlation function by

$$C(q) = \frac{A_{12}(q)}{B_{12}(q)}, \quad (4)$$

where $A_{12}(q)$ is for the number of pairs from the same event while $B_{12}(q)$ is constructed from mixed events. Equation (4) is related to the two-particle and single-particle spectra as

$$C(q) = \frac{\int \frac{d\mathbf{p}_1}{E_1} \frac{d\mathbf{p}_2}{E_2} N_{12}(\mathbf{p}_1, \mathbf{p}_2) \delta(q - \sqrt{-q^2})}{\int \frac{d\mathbf{p}_1}{E_1} \frac{d\mathbf{p}_2}{E_2} N_1(\mathbf{p}_1) N_2(\mathbf{p}_2) \delta(q - \sqrt{-q^2})}, \quad (5)$$

where the momentum integration should reflect the experimental momentum coverage.

The source function $S_i(x, \mathbf{p})$ is defined as the phase-space distribution of the particles at freeze-out and is related to the single-particle spectrum as

$$N_i(\mathbf{p}) = \int d^4x S_i(x, \mathbf{p}). \quad (6)$$

Then the two-particle spectrum from uncorrelated (chaotic) sources reads

$$N_{12}(\mathbf{p}_1, \mathbf{p}_2) \simeq \int d^4x d^4y S_1(x, \mathbf{p}_1) S_2(y, \mathbf{p}_2) |\Psi(x, y, \mathbf{p}_1, \mathbf{p}_2)|^2, \quad (7)$$

$$\simeq \int d^4x d^4y S_1(x, \mathbf{p}_1) S_2(y, \mathbf{p}_2) |\varphi(\mathbf{q}^*, \mathbf{r}^*)|^2, \quad (8)$$

where $\Psi(x, y, \mathbf{p}_1, \mathbf{p}_2)$ denotes the Bethe-Salpeter amplitude describing propagations of pairs from the emission point x and y to the asymptotic state with momenta \mathbf{p}_1 and \mathbf{p}_2 . The squared two-particle amplitude is well approximated by the relative wave function $\varphi(\mathbf{q}^*, \mathbf{r}^*)$ in the pair rest frame defined by $\mathbf{P} = 0$. Here \mathbf{q}^* and $\mathbf{r}^* = \mathbf{x}^* - \mathbf{y}^*$ are the spatial components of relative momentum and the relative coordinate defined in

the pair rest frame, respectively. Note that $q = |\mathbf{q}^*|$ when $\mathbf{P} = 0$. The information on the pairwise interaction is encoded in $\varphi(\mathbf{q}^*, \mathbf{r}^*)$, which can be obtained by solving the Schrödinger equation. The squared relative wave function $|\varphi(\mathbf{q}^*, \mathbf{r}^*)|^2$ can be viewed as a weight factor for the two-particle emission. Therefore $N_{12}(\mathbf{p}_1, \mathbf{p}_2)$ reduces to the product $N_1(\mathbf{p}_1)N_2(\mathbf{p}_2)$ for $|\varphi(\mathbf{q}^*, \mathbf{r}^*)|^2 = 1$. Note that Eq. (7) is valid under the chaotic source assumption, the so-called smoothness assumption [$S_i(x, \mathbf{p})$ being smooth in the momentum space], and the negligible correlation with other particles. The validity of Eq. (8) further requires \mathbf{q}^* to be small compared with the particle masses in order for $\varphi(\mathbf{q}^*, \mathbf{r}^*)$ to be regarded as the relative wave function. (See Refs. [22] for detailed discussion.)

If the center-of-mass coordinate and relative time are integrated, we obtain the Koonin-Pratt formula,

$$C^{(\text{KP})}(q) = \int d\mathbf{r}^* S_{12}^{\text{rel}}(\mathbf{r}^*) |\varphi(\mathbf{q}^*, \mathbf{r}^*)|^2, \quad (9)$$

where the relative source function $S_{12}^{\text{rel}}(\mathbf{r}^*)$ can be viewed as the relative source distribution in the pair rest frame. The relative source function is momentum dependent when the emission point is correlated with momentum, as is the case for collective expansion.

In this paper, we adopt a parameterized model of $S_i(x, \mathbf{p})$ with hydrodynamic expansion [23] with the parameters constrained from single-particle spectra through Eq. (6). Detailed analyses of π - π correlations at RHIC have revealed that various features of the expanding matter need to be implemented to produce the pion emitting source compatible with measurements [24]. Therefore, our parameterized source may be an oversimplification. On the other hand, precise shape of the source function is not crucially important in our one-dimensional correlation. Use of more realistic source functions through the implementations of state-of-the-art dynamical models will be left for future studies.

B. Correlations from S-wave scattering

Due to the short-range nature of the strong interaction, the modification of the relative wave function of nonidentical particle pairs takes place mainly in the S-wave state. Thus, one may express

$$\varphi(\mathbf{q}, \mathbf{r}) = e^{i\mathbf{q}\mathbf{r}} - j_0(|\mathbf{q}|\mathbf{r}) + \psi_{|\mathbf{q}|}(\mathbf{r}), \quad (10)$$

where $j_0(x)$ is the zeroth-order spherical Bessel function and $\psi_{|\mathbf{q}|}(\mathbf{r})$ is the S-wave relative wave function with the pairwise interaction effects. The connection of the pairwise interaction with the correlation function can be nicely illustrated by employing a static and spherically symmetric source function, $S_{12}^{\text{rel}}(\mathbf{r}^*) = S(r = |\mathbf{r}^*|)$, as Ref. [17]

$$C^{(\text{KP})}(q) = 1 + \int [d\mathbf{r}^*] [|\psi_q(\mathbf{r})|^2 - |j_0(q\mathbf{r})|^2], \quad (11)$$

where $[d\mathbf{r}^*] = d\mathbf{r}^* S(r)$ with $S(r)$ being properly normalized as $\int [d\mathbf{r}^*] = 1$. One immediately finds that the deviation of the wave function from the noninteracting one is directly translated into the correlation function and that the relative source function acts as a weight factor at relative distance r .

Furthermore, when the source size is not too small compared to the interaction range, the integral is dominated by the contribution outside the interaction range such that the wave function can be approximated by its asymptotic form $\psi_q(r) \sim e^{-i\delta} \sin(qr + \delta)/(qr)$ with δ being the S -wave-scattering phase shift. Employing a Gaussian source $S(r) \propto \exp(-r^2/4R^2)$ and the effective range formula for small q ,

$$q \cot \delta \simeq -\frac{1}{a_0} + \frac{1}{2} r_{\text{eff}} q^2, \quad (12)$$

one can express the correlation function in terms of the scattering length a_0 and the effective range r_{eff} , which is known as the Lednický-Lyuboshits (LL) formula [25],

$$C^{(\text{LL})}(q) = 1 + \frac{|f(q)|^2}{2R^2} F_3\left(\frac{r_{\text{eff}}}{R}\right) + \frac{2\text{Re}f(q)}{\sqrt{\pi}R} F_1(2qR) - \frac{\text{Im}f(q)}{R} F_2(2qR). \quad (13)$$

Here $f(q) = (q \cot \delta - iq)^{-1}$ is the scattering amplitude, $F_1(x) = \int_0^x dt e^{t^2 - x^2}$, $F_2(x) = (1 - e^{-x^2})/x$, and $F_3(x) = 1 - x/(2\sqrt{\pi})$. Since the scattering length dominates the behavior of the phase shift at small q , this correlation function is mainly determined by the scattering length and the source size: For $r_{\text{eff}} = 0$, $C^{(\text{LL})}(q)$ is a function of two dimensionless variables, qR and R/a_0 [15].

Figure 1 represents characteristics of the correlation function $C^{(\text{LL})}(q)$ with $r_{\text{eff}} = 0$. For a fixed qR [Fig. 1(a)], the correlation function exhibits nonmonotonic changes against the ratio of the system size to the scattering length. It shows a strong peak around $R/a_0 \sim 0$ for small qR due to the strong enhancement of the wave function. We call the region where $C(q)$ is enhanced as the ‘‘unitary region’’ throughout this paper. The peak is smeared as qR is increased. As the attraction becomes weaker ($a_0 < 0$), the correlation is also weakened to exhibit monotonic decrease with decreasing R/a_0 and increasing qR . On the other hand, if the attraction is strong enough to accommodate a bound state ($a_0 > 0$), $C(q)$ rapidly decreases with R/a_0 and then takes values less than unity, implying the depletion of correlated pairs at small qR . The depletion can be understood by the so-called structural core; the scattering wave function needs to be orthogonal to the bound-state wave function, and then it has a node in the interaction range as if there is a repulsive core. Thus the squared wave function is suppressed on average.

The above properties of $C(q)$ are essential in order to extract the pairwise interaction from the measured correlation functions. In particular, the behavior of $C(q)$ for different system size provides detailed information on the scattering parameters as shown in Fig. 1(b). Consider the case where $C(q) \gg 1$ at small qR . It indicates that the system is in the unitary region where $|R/a_0|$ is small, while the sign of a_0 is unknown. However, by increasing R with a_0 and qR fixed, $C(q)$ eventually becomes smaller than 1 for positive a_0 , while $C(q)$ is always larger than 1 for negative a_0 .

In reality, the correlation at small q originates not only from the single-channel FSI but also from the quantum statistics in the case of identical pairs (Hanbury Brown-Twiss (HBT) effect), from the Coulomb interaction, and from the coupled-

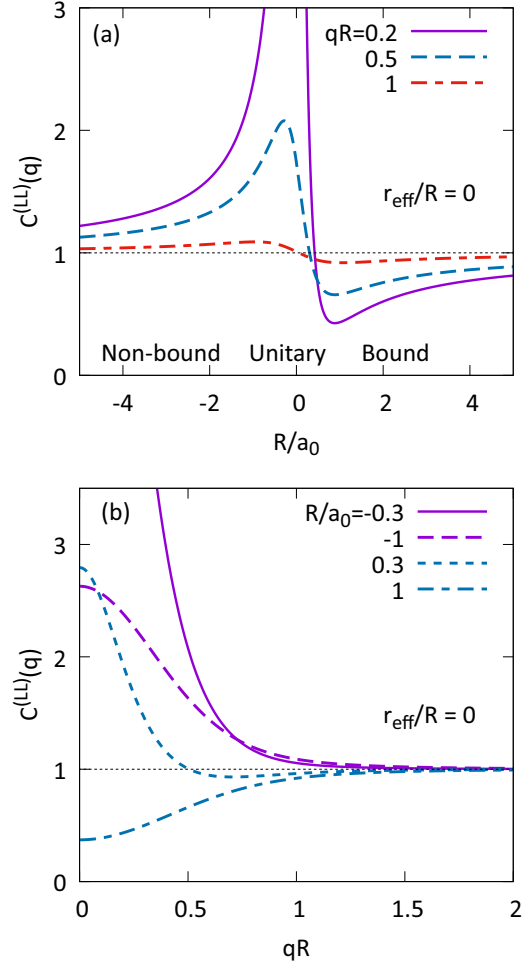


FIG. 1. The correlation function $C^{(\text{LL})}(q)$ with $r_{\text{eff}} = 0$ as a function of R/a_0 for different qR (a) and as a function of qR for different R/a_0 value (b). In the present sign convention, $a_0 > 0$ corresponds to the existence of a bound state.

channels effect [26]. Furthermore, the correlation from the HBT effect is affected by the collective flow through the modification of the source geometry. As a result, even for non-identical pairs, the absolute magnitude of $C(q)$ with respect to unity is not always a useful measure to quantify the effect of FSI in heavy-ion collisions. However, by taking a ratio of the correlation functions with small and large system sizes as

$$C_{\text{SL}}(q) = C_{\text{small-}R}(q)/C_{\text{large-}R}(q), \quad (14)$$

one can nicely cancel out the effect of the Coulomb interaction between charged pairs and extract the FSI from the strong interaction, as demonstrated in Ref. [17]. We will follow this idea in this paper to study $\Omega\Omega$ and $p\Omega$ correlations.

III. MODELING EMISSION FUNCTION

As seen from Fig. 1, the correlation from FSI strongly depends on the source size. In order to extract the pairwise interaction from the correlation function, one needs to know the source size or to look at the system size dependence of the correlation [17]. Therefore, modeling the particle source is

one of the indispensable ingredients in quantitative analyses. Here we employ a thermal source model with hydrodynamic expansion in which parameters are so tuned as to reproduce relevant particle yields and spectra.

We assume that the baryon production takes place at chemical and thermal freeze-out temperature T_f from a cylindrically expanding boost-invariant fireball, where the flow velocity $u^\mu(x)$ is parameterized as $u^\mu = (\cosh \eta_s \cosh y_T, \sinh y_T \cos \phi, \sinh y_T \sin \phi, \sinh \eta_s \cosh y_T)$ with $\eta_s = \tanh^{-1}(z/t)$ being the space-time rapidity. The transverse rapidity y_T is parameterized as $y_T = \alpha(r_T/R_T)^\beta$, where α and β are the fitting parameters and R_T denotes the transverse source size. Then the emission function of particle species i can be written as [23]

$$d^4x S_i(x, \mathbf{p}) = \tau_0 d\eta_s d^2r_T \frac{d}{(2\pi)^3} n_F(u \cdot p, T) \exp\left(-\frac{r_T^2}{2R_T^2}\right), \quad (15)$$

where \mathbf{p} is the on-shell momentum, x is the space-time emission point, d denotes the spin degeneracy, and n_F denotes the Fermi distribution function. We assume that hadrons are produced at a constant proper time $\tau = \sqrt{t^2 - z^2} = \tau_0$ with a Gaussian profile in the transverse direction. The use of azimuthally symmetric profile is an oversimplification since it does not account for the significant anisotropic flow in noncentral events, but we retain it in order to reduce the number of parameters. In fact, the one-dimensional baryon-baryon correlation functions are not expected to be strongly sensitive to detailed source shape in the transverse plane, since it can be expressed in terms of relative source distribution (9). By integrating over η_s and r_T , one obtains the single-particle spectrum, $E dN/d^3p$. In the Boltzmann approximation $m \gg T$, the thermal spectrum is proportional to the volume factor $V = 2\pi \tau_0 R_T^2$, so that we have

$$\frac{dN}{dy p_T dp_T 2\pi} = \frac{d}{(2\pi)^3} 2m_T V \int_0^\infty d\rho e^{-\rho^2/2} \times I_0\left(\frac{p_T}{T} \sinh y_T\right) K_1\left(\frac{m_T}{T} \cosh y_T\right), \quad (16)$$

where I_0 and K_1 are the modified Bessel functions.

The parameters in our model are determined by the following procedure. First, we fix the freeze-out temperature to $T_f = 155$ MeV from the fit to the various particle multiplicity data at the Large Hadron Collider (LHC) [29]. We perform a fit to the experimental transverse-momentum spectra of each species by varying three parameters (V , α , and β). Finally, we fix $\tau_0 = 10$ fm/c from a freeze-out temperature in a hydrodynamic model calculation [30] for the most central event bin (5–10%) in Ω production analyses [27]. We take the relation $\tau_0 \simeq (dN/dy)^{1/3}$ which is expected from the property of longitudinal HBT radii $R_{\text{long}} \simeq \tau_0 \sqrt{T_f/m_T}$ [31] and well-established relation between the HBT radii and multiplicity. Then R is obtained from the fitted values of the volume factor V .

Figure 2 displays the fitted transverse-momentum spectra for Ω s and protons. The obtained parameter sets are summarized in Table I. We take into account two-body decay contributions from resonances with mass $m_R < 2$ GeV to the

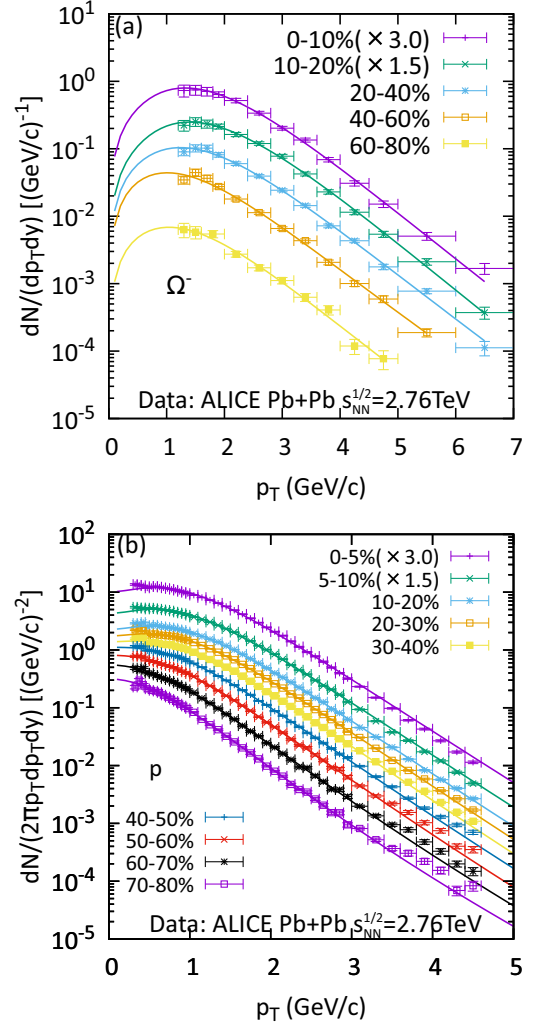


FIG. 2. Transverse-momentum spectra of (a) Ω and (b) p . Experimental data are taken from Refs. [27] and [28] for Ω and protons, respectively. Two most central events are scaled by factor 3 and 1.5 for better comparison.

proton spectra. We note that those resonance contributions are important to fit the total yield of protons with reasonable system sizes. Note also that there is so-called thermal proton yield anomaly at LHC [29]. (See Ref. [32] for a possible resolution.) The proton spectra have more detailed centrality bins than those of the Ω , such that fits are made for those data. In the calculations of the correlation function below, we

TABLE I. Parameters in the emission function (15) for different centralities and particle species.

Centrality	τ_0 (fm/c)	R_T^Ω (fm)	R_T^p	α^Ω	β^Ω	α^p	β^p
0–10%	10.0	8.0	6.8	0.584	0.628	0.759	0.421
10–20%	9.085	6.75	6.23	0.618	0.579	0.750	0.425
20–40%	7.5	5.88	5.2	0.546	0.692	0.707	0.466
40–60%	5.5	4.38	3.92	0.444	0.858	0.604	0.6
60–80%	3.62	2.12	2.66	0.456	0.812	0.456	0.82

adjust the centrality selections to Ω data. Thus, the parameters shown in Table I are those used in the subsequent calculations and are obtained by averaging over corresponding centralities in the spectrum (i.e., 0–10% parameters are obtained by averaging 0–5% and 5–10% with multiplicity being the weight.) Clearly, the present model is too simple to fully account for other possible contributions to the proton spectrum such as rescattering effect after chemical freeze-out. Nevertheless, we have checked that proton HBT radii from the model are consistent with measurements [33]. Therefore, we expect that the following results remain valid for more realistic modeling of the particle sources.

IV. $\Omega\Omega$ CORRELATION

First we discuss pairs of $\Omega(1672)$ particles. A recent LQCD calculation shows that the $J = 0$ $\Omega\Omega$ system has a shallow bound state [12]. Direct detection of the $\Omega\Omega$ dibaryons (di-Omega) is highly challenging because of the tiny production rate for the $S = -6$ object even in heavy-ion collisions and the background yields of the decay products would be high. On the other hand, the high-luminosity upgrade at the LHC may allow for measuring the momentum correlation of $\Omega\Omega$ pairs in the future.

A. $\Omega\Omega$ interaction from lattice QCD

Since Ω has a spin $3/2$, the $\Omega\Omega$ pairs can have $J = 0, 1, 2$, and 3 . Among others, the $J = 0$ state is expected to have appreciable S -wave attraction without suffering from the Pauli exclusion effect for valence quarks. The interaction potential $V_{\Omega\Omega}^{J=0}$ was recently calculated by (2+1)-flavor lattice QCD simulations [12] with a large lattice volume $(8.1 \text{ fm})^3$, a small lattice spacing $a \simeq 0.0846 \text{ fm}$ and nearly physical quark masses ($m_\tau \simeq 146 \text{ MeV}$, $m_K \simeq 525 \text{ MeV}$, $m_N \simeq 964 \text{ MeV}$, and $m_\Omega \simeq 1712 \text{ MeV}$). In the time-dependent HAL QCD method [10] employed in the analysis, the lattice data at moderate values of the Euclidean time, $t \sim (1 - 2) \text{ fm}$, are found to be sufficient to extract the baryon-baryon interaction. For $\Omega\Omega$, the interval $t/a = 16\text{--}18$ is chosen to avoid the contamination from the excited state of a single Ω at small t and large statistical errors at large t .

Resultant potentials with statistical errors are recapitulated in Fig. 3 together with the fitted potential of the three-range Gaussian form [12]. The scattering length and the effective range without the Coulomb repulsion are $a_0 \simeq 4.6 \text{ fm}$ and $r_{\text{eff}} \simeq 1.27 \text{ fm}$, respectively, so that a weakly bound di-Omega appears with the binding energy $E_B \simeq 1.6 \text{ MeV}$.

Table II shows the low-energy-scattering parameters and binding energies obtained by solving the Schrödinger equation in the presence of the attraction from the strong interaction and the repulsion from the Coulomb interaction. The already large positive scattering length found in lattice QCD calculations is further driven toward the unitary limit ($a_0 \gg r_{\text{eff}}$) by the Coulomb repulsion. The obtained scattering length exceeds the effective source size in heavy-ion collisions; therefore one can expect the correlation function belongs to the unitary region characterized by $R/a_0 \sim 0$ in Fig. 1(a).

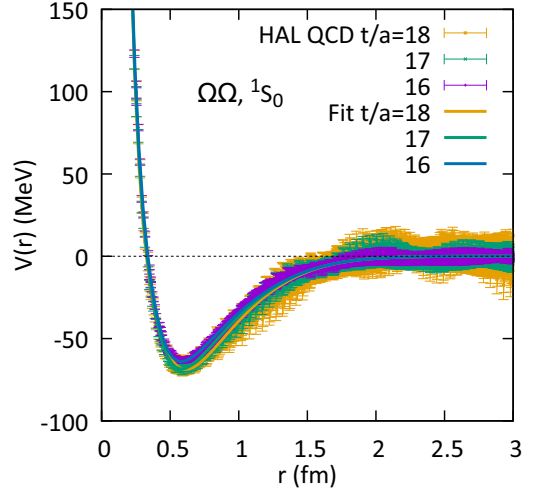


FIG. 3. The $\Omega\Omega$ potential in $J = 0$ channel from lattice QCD simulations [12]. The lattice data are fitted by the form, $V_{\text{fit}}(r) = \sum_{j=1,2,3} c_j e^{-(r/d_j)^2}$.

B. Correlation function

Assuming that the strong interaction except for the $J = 0$ channels is negligible, one may write the wave functions à la Eq. (10) with the Coulomb repulsion and the Fermi statistics (symmetrization for $J = 0, 2$ and antisymmetrization for $J = 1, 3$):

$$\varphi^{J=0}(\mathbf{q}, \mathbf{r}) = \varphi_{\text{sym}}^C(\mathbf{q}, \mathbf{r}) - \varphi_{0,\text{sym}}^C(r) + \chi_0^C(r), \quad (17)$$

$$\varphi^{J=2}(\mathbf{q}, \mathbf{r}) = \varphi_{\text{sym}}^C(\mathbf{q}, \mathbf{r}), \quad (18)$$

$$\varphi^{J=1,3}(\mathbf{q}, \mathbf{r}) = \varphi_{\text{asym}}^C(\mathbf{q}, \mathbf{r}). \quad (19)$$

Here $\varphi_{\text{sym}}^C(\mathbf{q}, \mathbf{r})$ and $\varphi_{\text{asym}}^C(\mathbf{q}, \mathbf{r})$ denote the Coulomb wave functions with symmetrization and antisymmetrization, respectively. Also, $\varphi_{0,\text{sym}}^C(r)$ is the S -wave component of $\varphi_{\text{sym}}^C(\mathbf{q}, \mathbf{r})$. The full wave function in the S -wave, $\chi_0^C(r)$, is obtained by solving the Schrödinger equation with the strong interaction potential $V_{\text{fit}}(r)$ in Fig. 3 together with the Coulomb repulsion. In the absence of the Coulomb interaction, these expressions reduce to the case of neutral particles, e.g., $\Lambda\Lambda$ pairs shown in Ref. [16]. Also note that the wave functions φ^J in Eqs. (17)–(19) contain the higher-partial wave ($L \geq 1$) components. The total probability density is thus given by

$$|\varphi_{\Omega\Omega}(\mathbf{q}, \mathbf{r})|^2 = \sum_{J=0}^3 \frac{2J+1}{16} |\varphi^J(\mathbf{q}, \mathbf{r})|^2. \quad (20)$$

TABLE II. Scattering length a_0 , effective range r_{eff} , and binding energy of the $\Omega\Omega$ pair with the lattice QCD potential for different t/a and the Coulomb repulsion.

t/a	a_0 (fm)	r_{eff} (fm)	E_B (MeV)
16	65.28	1.29	0.1
17	17.59	1.24	0.54
18	11.69	1.26	1.0

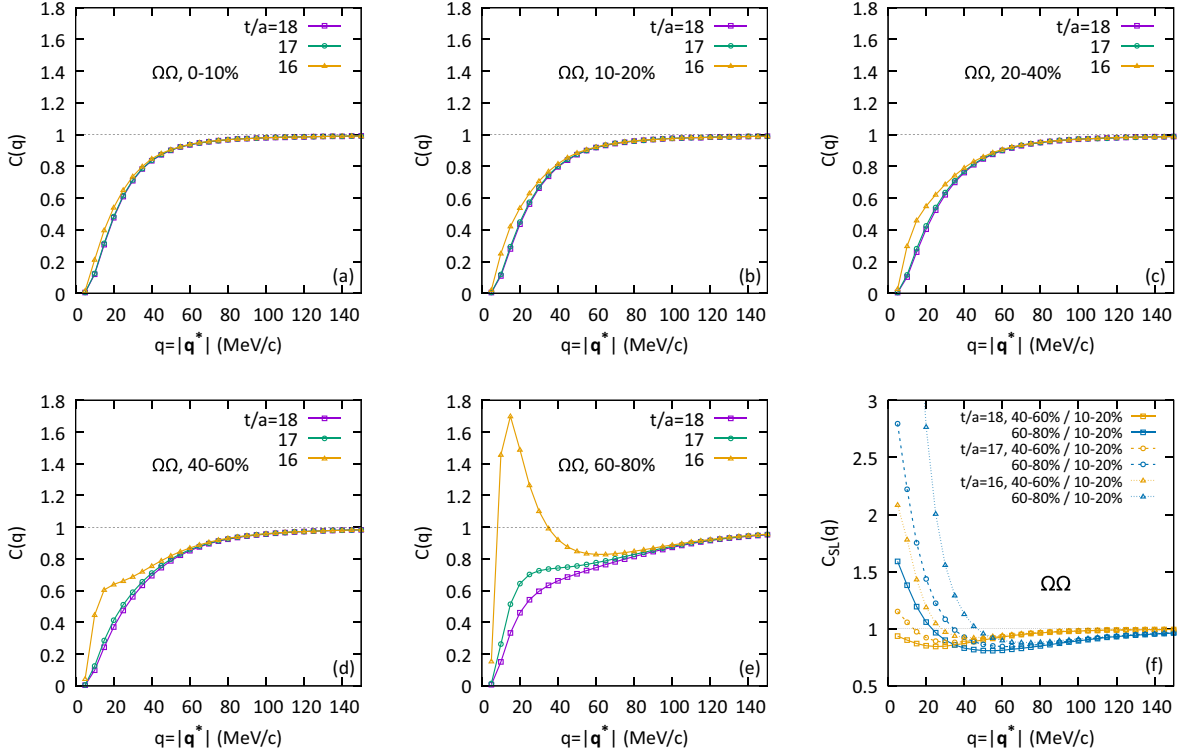


FIG. 4. $\Omega\Omega$ correlation function $C(q)$ from central (0–10%) to peripheral (60–80%) Pb-Pb collisions, as well as the small-to-large ratio $C_{SL}(q)$.

Note that the effect of the strong interaction in $J = 0$ is weighted only by $1/16$ in the probability.

We calculate the correlation function $C(q)$ in Eq. (5) by combining Eq. (15) and Eq. (20). In the momentum integral, we take vanishing particle rapidities and fix the transverse momentum to the average values obtained from the spectra (Fig. 2). In Fig. 4, $\Omega\Omega$ correlation functions for different centralities are displayed. Note that the system size becomes smaller as the centrality increases. The depletion of $C(q)$ below 1 at small q is due to the Coulomb repulsion and the HBT effect. Also the latter effect extends to wider region of q for smaller systems. As shown in a schematic analysis given in Fig. 1(b), the correlation function exhibits stronger FSI effect with decreasing system size. Such a tendency can be seen particularly for the $\Omega\Omega$ potential with $t/a = 16$ in Fig. 4, since a_0 is extremely large.

Shown in Fig. 4(f) is the small-to-large ratio, $C_{SL}(q)$, between 40–60% (or 60–80%) for small systems and 10–20% for large systems. Due to the cancellation of the Coulomb effect, one now finds notable enhancement of $C_{SL}(q)$ above 1 for small q due to the strong $\Omega\Omega$ attraction and the reduction of $C_{SL}(q)$ below 1 for large q due to the HBT effect.

V. $p\Omega$ CORRELATION

Let us now move on to the results for $p\Omega$ correlations. Among $J = 1$ (3S_2) and $J = 2$ (3S_1) channels which the $p\Omega$ pair can take, the $J = 2$ channel is expected to have a shallow bound state as indicated from lattice QCD [13]. Note, however, that the $p\Omega$ pair is not the lowest energy channel

in the $S = -3$ dibaryon system: There exist thresholds of the octet-octet states ($\Lambda\Xi$ and $\Sigma\Xi$) at lower energies, which act as absorptive channels for $p\Omega$. The S -wave $J = 2$ channel couples to octet-octet states only through the D -wave, so that the decay is dynamically suppressed and its effect on the correlation function is considered to be sufficiently small. According to Ref. [34], where the $J = 2$ $N\Omega$ interaction is discussed with the meson exchange model including the decay channels, the coupling does not change the weak-binding nature of $p\Omega$. Thus, in the following calculations, we apply the single-channel approximation to the $J = 2$ $p\Omega$ correlation function.

In the previous study on $C_{SL}(q)$ for $p\Omega$ [17], the $J = 2$ potential obtained by lattice QCD simulations with heavy quark masses [35] were used. Below we update the analysis by using the $J = 2$ potential for nearly physical quark masses as described below.

A. $N\Omega$ interaction from lattice QCD

The $N\Omega$ interaction in $J = 2$ channel has been calculated by (2+1)-flavor lattice QCD simulations [13] with the same setup as the $\Omega\Omega$ case discussed in Sec. IV A. In this case, the Euclidean time interval was chosen to be $t/a = 11 - 14$ to avoid significant statistical errors for large t . Resultant potentials with statistical errors are recapitulated in Fig. 5 together with the fitted potential of a Gaussian + (Yukawa)² form. The scattering length and the effective range without the Coulomb interaction are $a_0 \simeq 5.3$ fm and $r_{\text{eff}} \simeq 1.26$ fm,

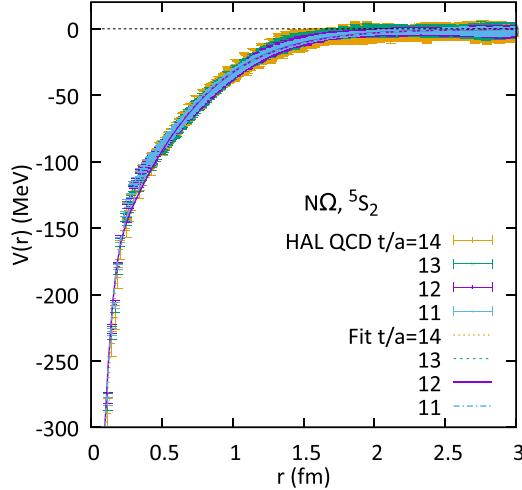


FIG. 5. The S -wave $N\Omega$ potential with $J = 2$ from lattice QCD simulations [13]. The lattice data are fitted by the form $V_{\text{fit}}(r) = b_1 e^{-b_2 r^2} + b_3 (1 - e^{-b_4 r^2})(e^{-m_\pi r}/r)^2$ with $m_\pi = 146$ MeV.

respectively, so that a weakly bound $N\Omega$ appears with the binding energy $E_B \sim 1.54$ MeV.

Table III shows the low-energy-scattering parameters and binding energies obtained by solving the Schrödinger equation in the presence of the attraction from the strong interaction and the extra attraction from the Coulomb interaction. The value of the resultant scattering length is compatible with the expected effective system size in heavy-ion collisions, thus one can expect characteristic depletion of the correlation function and its variation for the system with bound state, against system size as seen from Fig. 1.

B. Correlation function

In addition to the $J = 2$ channel, the $N\Omega$ system has the $J = 1$ channel which is expected to couple strongly with low-lying octet-octet states due to fall apart decay in the S -wave. In the same way as Ref. [17], we consider a limiting case where the $J = 1$ $p\Omega$ pairs are perfectly absorbed into low-lying states through the potential $V^{J=1}(r) = -i\theta(r_0 - r)V_0$. The strength V_0 is taken to be infinity and r_0 is set to 2 fm where Coulomb interaction dominates over the $J = 1$ LQCD potential. Accordingly, the wave function is written as $\varphi^J(\mathbf{q}, \mathbf{r}) = \varphi^C(\mathbf{q}, \mathbf{r}) - \varphi_0^C(r) + \chi_0^C(r)$, where the scattering wave function in the S -wave, $\chi_0^C(r)$, receives the effects of the interactions.

TABLE III. S -wave scattering length a_0 , effective range r_{eff} , and binding energy of the $p\Omega$ pair with the lattice QCD potential for different t/a and the Coulomb attraction.

t/a	a_0 (fm)	r_{eff} (fm)	E_B (MeV)
11	3.45	1.33	2.15
12	3.38	1.31	2.27
13	3.49	1.31	2.08
14	3.40	1.33	2.24

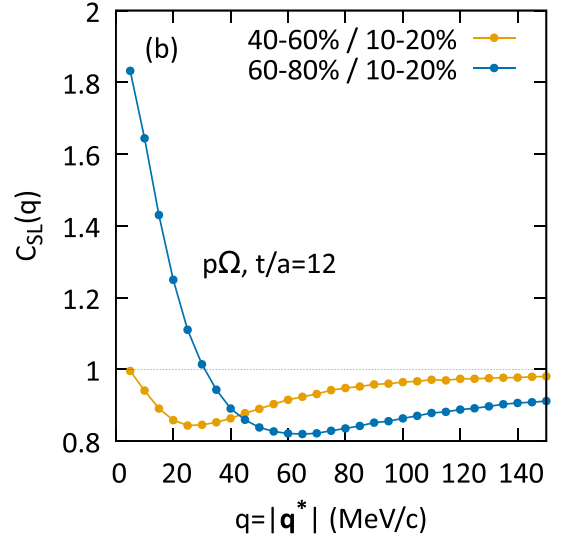
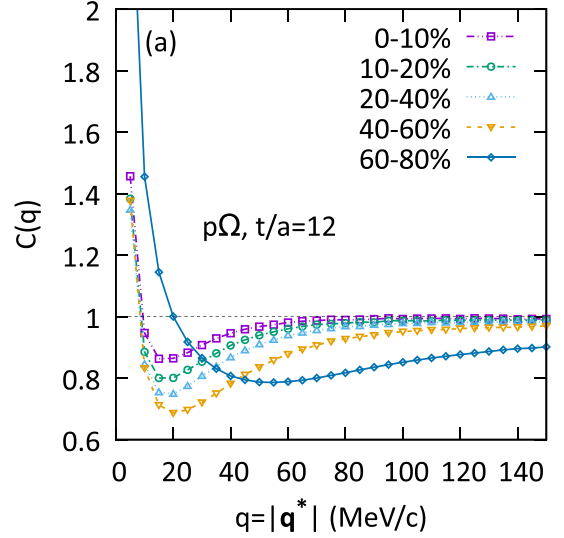


FIG. 6. $p\Omega$ correlation function from central (0–10%) to peripheral (60–80%) Pb-Pb collisions (a), as well as from peripheral to central collisions and the small-to-large ratio (b).

Then the total probability density reads

$$|\varphi_{p\Omega}(\mathbf{q}, \mathbf{r})|^2 = \sum_{J=1}^2 \frac{2J+1}{8} |\varphi^J(\mathbf{q}, \mathbf{r})|^2. \quad (21)$$

Here the $J = 2$ contribution which is of our interest, is weighted by a large factor $5/8$. The number of the low-momentum pairs decrease due to the absorption in the $J = 1$ channel and the resultant correlation function $C(q)$ tends to decrease but not with significant amount as discussed in Ref. [17].

Figure 6 shows the $p\Omega$ correlation functions from peripheral to central collisions. Since the $N\Omega$ potential in Fig. 5 is nearly independent of t/a , the same holds for $C(q)$, too. Thus we display only results of $t/a = 12$. The enhancement of $C(q)$ above 1 for small q is due to the Coulomb attraction, whereas the suppression of $C(q)$ below 1 is due to the positive

scattering length or, equivalently, the existence of $p\Omega$ bound state. The effect of FSI is smallest (largest) in central collisions (0–10%) [peripheral collisions (60–80%)], so that the region of the suppressed correlation becomes deeper and wider as the system size decreases, in accordance with the moderate value of the scattering length ($a_0 \simeq 3.4$ fm) in Table III.

Shown in Fig. 6(b) is the small-to-large ratio, $C_{SL}(q)$, between 40–60% (or 60–80%) for the small system and 10–20% for the large system. After the cancellation of the Coulomb effect, one now finds notable enhancement of $C_{SL}(q)$ above 1 at small q and depletion below 1 at $q = (20\text{--}80)$ MeV due to the strong $p\Omega$ attraction accommodating a bound state. In response to the theoretical proposal in Ref. [17], the STAR collaboration at RHIC has reported a first measurement of $p\Omega$ correlation in Au+Au collisions [20]. Although the statistics of the data are not sufficient to draw a definitive conclusion, the measured $C(q)$ and $C_{SL}(q)$ show similar tendency with Fig. 6 in the present paper.

VI. SUMMARY AND CONCLUDING REMARKS

We have studied the two-particle momentum correlations for $\Omega\Omega$ and $p\Omega$ in relativistic heavy-ion collisions. The correlation functions are calculated by using an expanding source model combined with the latest lattice QCD potentials which predict shallow bound states with relatively large positive scattering lengths in the $J = 0$ $\Omega\Omega$ and the $J = 2$ $N\Omega$.

At the LHC energies, the correlation function $C(q)$ for $\Omega\Omega$ in Pb-Pb collisions exhibits an enhancement due to large scattering length ($a_0 > 10$ fm) over the Coulomb repulsion and the HBT effect, especially in the peripheral events. This characteristic feature can be best visible and quantified as an enhancement of the small-to-large ratio $C_{SL}(q)$ at $q < 40$ MeV/ c .

On the other hand, the characteristic feature of the correlation function $C(q)$ of $p\Omega$ is its depletion below 1 at $q = 20\text{--}40$ MeV due to the moderately large value of the positive scattering length $a_0 \simeq 3.4$ fm. Properly chosen small-to-large ratio $C_{SL}(q^*)$ also exhibits this behavior.

Measuring the $\Omega\Omega$ in heavy-ion collisions is a challenge even with the high-luminosity upgrade of LHC due to its small production rate as well as the correlation measurement at small q (< 50 MeV). Therefore, not only the luminosity upgrade but also the improvements of measurement techniques would be necessary.

In response to our theoretical proposal in Ref. [17], the STAR collaboration at RHIC has reported a first measurement of $p\Omega$ correlation in Au+Au collisions [20]. Although the statistics of the data are not sufficient to draw a definitive conclusion, the measured $C(q)$ and $C_{SL}(q)$ show similar tendency with Fig. 6 in the present paper. Also the ALICE Collaboration at LHC has started the $p\Omega$ measurements with pp and p -Pb collisions [36]. Extracting the $p\Omega$ interaction from a combined theoretical analysis of the pp , pA , and AA collisions with proper uncertainty quantification would be an interesting future problem. (See Appendix A for an exploratory study along such direction.)

In order to draw definite conclusion on the existence of the $\Omega\Omega$ and $N\Omega$ dibaryon bound states from the future and

existing correlation function data, we need further works to be done. First, it is desired to obtain not only the $J = 0$ $\Omega\Omega$ potential and $J = 1$ $N\Omega$ potential but also the $J = 1, 2$ and 3 $\Omega\Omega$ potentials and the $J = 1$ $N\Omega$ potential. Second, the coupled channel effects need to be clarified. As discussed in Appendix A, the $J = 1$ contribution causes visible uncertainties in the $p\Omega$ correlation function. While the coupling effects to octet-octet channels with $J = 1$ in the $p\Omega$ correlation function have been assumed to be described by the absorption, the coupled-channels formula [26] shows that creation processes such as $\Lambda \Xi \rightarrow p\Omega$ also contribute to the correlation function of $p\Omega$. Then we need to evaluate the transition potentials and the source function of Λ and Σ .

ACKNOWLEDGMENTS

The authors thank Takumi Iritani and Takumi Doi for useful discussions and valuable help in preparing the manuscript. The authors also thank Sinya Aoki, Kenji Sasaki, Neha Shah, Laura Fabbietti, Valentina Mantovani Sarti, Otón Vázquez Doce, Johann Haidenbauer, and other participants of the YITP workshop (YITP-T-18-07) for useful discussions. This work is supported in part by the Grants-in-Aid for Scientific Research from JSPS (Grants No. 19H05151, No. 19H05150, No. 19H01898, No. 18H05236, and No. 16K17694), by the Yukawa International Program for Quark-hadron Sciences (YIPQS), by the Polish National Science Center NCN under Maestro Grant No. DEC-2013/10/A/ST2/00106, by the National Natural Science Foundation of China (NSFC) and the Deutsche Forschungsgemeinschaft (DFG) through the funds provided to the Sino-German Collaborative Research Center “Symmetries and the Emergence of Structure in QCD” (NSFC Grant No. 11621131001 and DFG Grant No. TRR110), by the NSFC under Grants No. 11747601 and No. 11835015, and by the Chinese Academy of Sciences (CAS) under Grants No. QYZDB-SSW-SYS013 and No. XDPB09.

APPENDIX A: SYSTEM-SIZE DEPENDENCE OF $C(q)$ FOR $p\Omega$ WITH UNCERTAINTY QUANTIFICATION

In the light of feasibility of measuring $p\Omega$ correlation in pp , pA , and AA collisions, it is desirable to get a feel for theoretical uncertainties in evaluating the momentum correlations. In the following, we focus on the uncertainties originating from the $J = 2$ $p\Omega$ potential from lattice QCD and from the treatment of the unknown $J = 1$ $p\Omega$ potential. To make the discussion transparent, we consider a simplified static and spherically symmetric Gaussian source function $S(r) = (4\pi R^2)^{-3/2} \exp(-r^2/4R^2)$ with the source size ranging from 0.8 to 4 fm.

For uncertainties arising from the insufficient information on the $J = 1$ potential, we evaluate “minimum” and “reference” contributions from the $J = 1$ channel. The “minimum” is obtained by assuming $\chi_0^{C,J=1}(r) = 0$, i.e., complete absorption of the wave function in all range of r . This leads to the minimum value of $C(q)$ as seen in Eq. (11). The “reference” is obtained by assuming $\chi_0^{C,J=1}(r) = \chi_0^{C,J=2}(r)$, i.e., the same attraction between $J = 1$ and $J = 2$ without absorption. The statistical uncertainty for each case is estimated by the

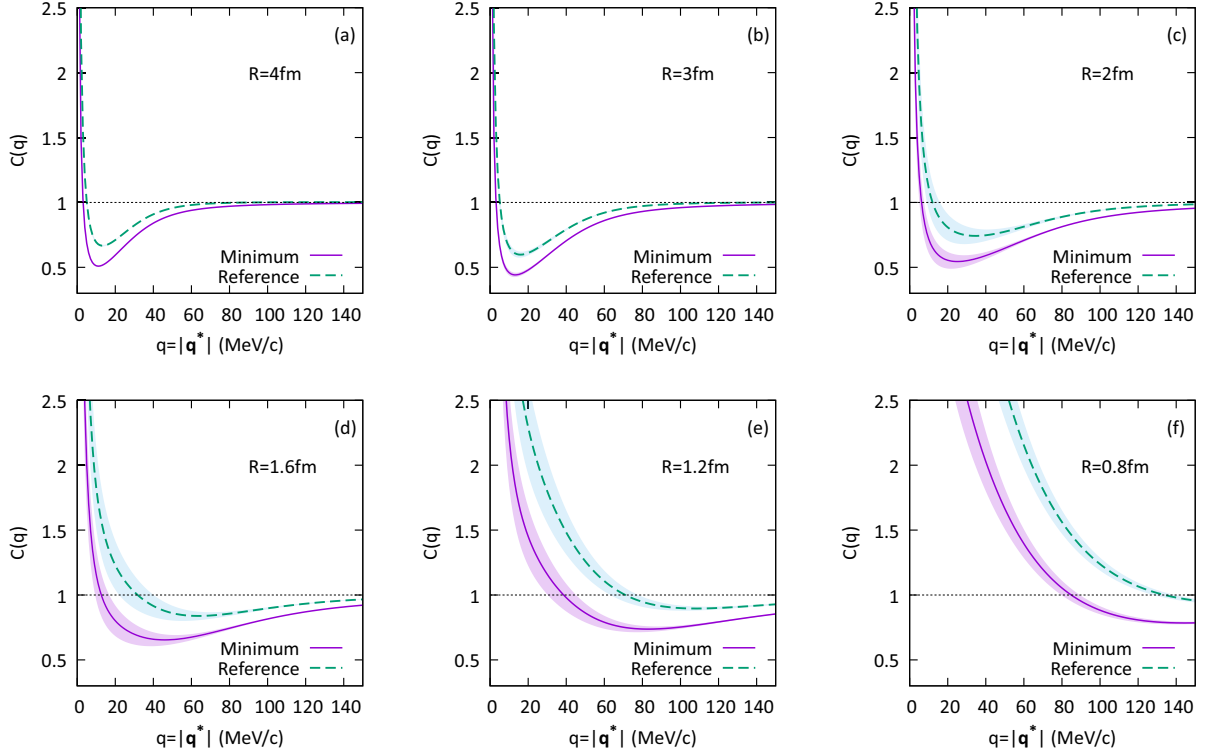


FIG. 7. $p\Omega$ correlation function calculated with the static Gaussian source function employing the $t/a = 12$ potential. The purple solid line denotes the result with $\chi_0^{C,J=1} = 0$, and blue dashed line denotes the result with the assumption of $\chi_0^{C,J=1} = \chi_0^{C,J=2}$. Gaussian source size is chosen to be in the range $R = 0.8\text{--}4$ fm. The error of each correlation estimated with the Jackknife method is shown by the colored shadow.

statistical error of the $J = 2$ $N\Omega$ potential at $t/a = 12$ by the Jackknife method in the similar way as in Ref. [13].

The results of $C(q)$ for different values of R are shown in Fig. 7. The shaded areas represent the statistical errors obtained from the Jackknife analysis. For $R \leq 2$ fm, the “minimum” and “reference” correlation functions exhibit sizable differences with larger statistical uncertainty. This is because the condition for the unitary region shown in Fig. 1 begins to hold with $a_0 \simeq 3.4$ fm in Table III), so that the correlation function becomes more sensitive to the uncertainty of the potential as well as the treatment of the $J = 1$ channel.

Within the above uncertainty estimate, we can safely conclude that the correlation function can be strongly suppressed at $q < 40$ MeV for systems with $2 \text{ fm} \lesssim R \lesssim 4 \text{ fm}$. We also find that the suppressed region of $C(q)$ moves toward the lower q direction with increasing source size. This behavior is consistent with the trend found in the data from Au+Au collisions by the STAR Collaboration at RHIC [20]. By comparison, strong enhancement at small momenta would be observed for small systems with $R \simeq 1$ fm as found in the preliminary data by the ALICE Collaboration at LHC [36].

APPENDIX B: COMPARISON OF $N\Omega$ POTENTIALS

We here compare the $J = 2$ $N\Omega$ potential used in this work and those used in Ref. [17]. The former is obtained from LQCD simulations with nearly physical quark masses ($m_\pi = 146$ MeV and $m_K = 525$ MeV) [13], while the latter is those with heavier quark masses ($m_\pi = 875$ MeV and

$m_K = 916$ MeV) [35]. In Fig. 8, we show the $J = 2$ $N\Omega$ potential with nearly physical quark masses at $t/a = 12$ (solid curve), and the potentials given in Ref. [17], V_I (dashed), V_{II} (dotted), and V_{III} (dash-dotted). The potential V_{II} is the best fit of the lattice data with heavier quark masses with

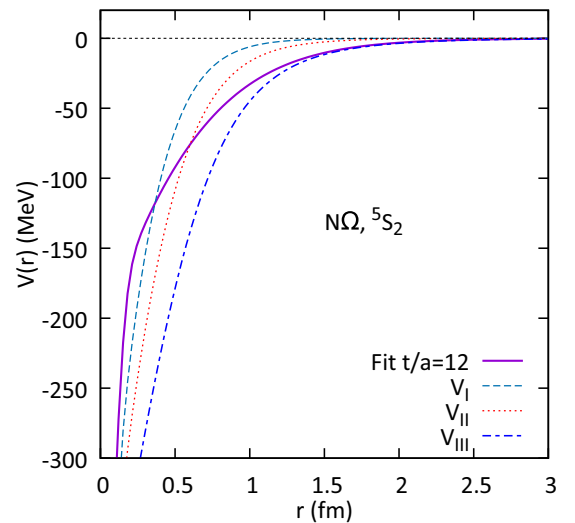


FIG. 8. Comparison of the S -wave $N\Omega$ potentials with $J = 2$ in Refs. [13] and [17]. The solid curve show the $N\Omega$ potential with nearly physical quark masses [13] at $t/a = 12$. The dashed, dotted, and dash-dotted curves show the $J = 2$ $N\Omega$ potentials, V_I , V_{II} , and V_{III} , given in Ref. [17].

a form $V_{\text{fit}}(r) = b_1 e^{-b_2 r^2} + b_3 (1 - e^{-b_4 r^2})(e^{-b_5 r}/r)^2$. V_{I} and V_{III} are two typical examples with weaker and stronger attractions, respectively. These potentials together with the Coulomb potential give no bound state for V_{I} , a shallow bound state $E_B \simeq 0.63$ MeV for V_{II} , and a deep bound state $E_B \simeq 26.9$ MeV for V_{III} . It should be noted that there is a typo in the binding energy with V_{II} +Coulomb potential in the original version of Ref. [17]. The value of 6.3 MeV shown

in Table I of Ref. [17] should be corrected to 0.63 MeV as updated in the erratum.

We find that the potential with nearly physical quark masses is between V_{II} and V_{III} ; the attraction becomes stronger with smaller quark masses, but not as attractive as V_{III} . Consequently, the $p\Omega$ correlation function shown in this work is also between those with V_{II} and V_{III} shown in Ref. [17].

-
- [1] A. Gal, *Acta Phys. Pol. B* **47**, 471 (2016).
 [2] H. Clement, *Prog. Part. Nucl. Phys.* **93**, 195 (2017).
 [3] H. C. Urey, F. G. Brickwedde, and G. M. Murphy, *Phys. Rev.* **39**, 164 (1932).
 [4] W. Rarita and J. Schwinger, *Phys. Rev.* **59**, 436 (1941).
 [5] R. L. Jaffe, *Phys. Rev. Lett.* **38**, 195 (1977); **38**, 617(E) (1977).
 [6] T. Goldman, K. Maltman, G. J. Stephenson, Jr., K. E. Schmidt, and F. Wang, *Phys. Rev. Lett.* **59**, 627 (1987).
 [7] M. Oka, *Phys. Rev. D* **38**, 298 (1988).
 [8] V. B. Kopeliovich, B. Schwesinger, and B. E. Stern, *Phys. Lett. B* **242**, 145 (1990).
 [9] N. Ishii, S. Aoki, and T. Hatsuda, *Phys. Rev. Lett.* **99**, 022001 (2007); S. Aoki, T. Hatsuda, and N. Ishii, *Prog. Theor. Phys.* **123**, 89 (2010).
 [10] N. Ishii, S. Aoki, T. Doi, T. Hatsuda, Y. Ikeda, T. Inoue, K. Murano, H. Nemura and K. Sasaki (HAL QCD Collaboration), *Phys. Lett. B* **712**, 437 (2012).
 [11] T. Doi and M. G. Endres, *Comput. Phys. Commun.* **184**, 117 (2013).
 [12] S. Gongyo *et al.* (HAL QCD Collaboration), *Phys. Rev. Lett.* **120**, 212001 (2018).
 [13] T. Iritani *et al.* (HAL QCD Collaboration), *Phys. Lett. B* **792**, 284 (2019).
 [14] S. Cho *et al.* (ExHIC Collaboration), *Phys. Rev. Lett.* **106**, 212001 (2011); *Phys. Rev. C* **84**, 064910 (2011).
 [15] S. Cho *et al.* (ExHIC Collaboration), *Prog. Part. Nucl. Phys.* **95**, 279 (2017).
 [16] K. Morita, T. Furumoto, and A. Ohnishi, *Phys. Rev. C* **91**, 024916 (2015).
 [17] K. Morita, A. Ohnishi, F. Etminan, and T. Hatsuda, *Phys. Rev. C* **94**, 031901(R) (2016); **100**, 069902(E) (2019).
 [18] A. Ohnishi, K. Morita, K. Miyahara, and T. Hyodo, *Nucl. Phys. A* **954**, 294 (2016).
 [19] T. Hatsuda, K. Morita, A. Ohnishi, and K. Sasaki, *Nucl. Phys. A* **967**, 856 (2017).
 [20] J. Adam *et al.* (STAR Collaboration), *Phys. Lett. B* **790**, 490 (2019).
 [21] M. A. Lisa, S. Pratt, R. Soltz, and U. Wiedemann, *Annu. Rev. Nucl. Part. Sci.* **55**, 357 (2005).
 [22] D. Anchishkin, U. W. Heinz, and P. Renk, *Phys. Rev. C* **57**, 1428 (1998); R. Lednicky, *Phys. Part. Nuclei* **40**, 307 (2009).
 [23] T. Csorgo and B. Lorstad, *Phys. Rev. C* **54**, 1390 (1996); S. Chapman, P. Scotto, and U. Heinz, *APH N.S., Heavy Ion Phys.* **1**, 1 (1995).
 [24] S. Pratt, *Phys. Rev. Lett.* **102**, 232301 (2009).
 [25] R. Lednicky and V. L. Lyuboshits, *Sov. J. Nucl. Phys.* **35**, 770 (1982) [*Yad. Fiz.* **35**, 1316 (1981)].
 [26] J. Haidenbauer, *Nucl. Phys. A* **981**, 1 (2019).
 [27] B. B. Abelev *et al.* (ALICE Collaboration), *Phys. Lett. B* **728**, 216 (2014); **734**, 409(E) (2014).
 [28] B. Abelev *et al.* (ALICE Collaboration), *Phys. Rev. C* **88**, 044910 (2013).
 [29] A. Andronic, P. Braun-Munzinger, K. Redlich, and J. Stachel, *Nature* **561**321 (2018).
 [30] X. Zhu, F. Meng, H. Song, and Y. X. Liu, *Phys. Rev. C* **91**, 034904 (2015).
 [31] A. N. Makhlin and Y. M. Sinyukov, *Z. Phys. C* **39**, 69 (1988).
 [32] A. Andronic, P. Braun-Munzinger, B. Friman, P. M. Lo, K. Redlich, and J. Stachel, *Phys. Lett. B* **792**, 304 (2019).
 [33] J. Adam *et al.* (ALICE Collaboration), *Phys. Rev. C* **92**, 054908 (2015).
 [34] T. Sekihara, Y. Kamiya, and T. Hyodo, *Phys. Rev. C* **98**, 015205 (2018).
 [35] F. Etminan *et al.* (HAL QCD Collaboration), *Nucl. Phys. A* **928**, 89 (2014).
 [36] O. Vázquez Doce *et al.* (ALICE Collaboration), Precise tests of the hadron-hadron strong interaction via femtoscopy with ALICE (2019), oral presentation at Hadron2019.
- Correction:* The previously published Figure 8 contained incorrectly plotted potentials and has been replaced.